50th AIAA Aerospace Sciences Meeting including the New Horizons Forum and Aerospace Exposition
09 - 12 January 2012, Nashville, Tennessee
AIAA 2012-1080

The Effect of a Gust on the Flapping Wing Performance

Martin Jones[1] and Nail K. Yamaleev[2]
North Carolina A&T State University, Greensboro, NC 27411

The effect of a wind gust on the aerodynamic characteristics of a rigid wing undergoing insect-based flapping motion is studied numerically. The turbulent flow near the flapping wing is described by the 3-D unsteady compressible Reynolds-Averaged Navier-Stokes equations with the Spalart-Allmaras turbulence model. The governing equations are solved using a second-order node-centered finite volume scheme on a hexahedral body-fitted grid that rigidly moves along with the wing. A low-Mach-number preconditioner is used to accelerate the convergence at each time step. The effects of wind gust direction with respect to a wing orientation are investigated. Our numerical results show that the centimeter-scale wing considered in the present study is susceptible to strong downward wind gusts. In the case of frontal and side gusts, the flapping wing can alleviate the gust effect if the gust velocity is less or comparable with the wing tip velocity. For all cases considered, the thrust coefficient returns to its original baseline profile within one full stroke after the gust is removed, thus indicating that the flapping wing can effectively recover from wind gust fluctuations.

I. Governing equations and Numerical Scheme

The fully turbulent compressible flow near a wing undergoing an insect-based flapping motion is simulated using the 3-D unsteady Reynolds-Averaged Navier-Stokes (URANS) equations written in the integral conservation law form as follows:

$$\frac{\partial (V\mathbf{Q})}{\partial t} + \oint_{\Gamma} (\mathbf{F}_i - \mathbf{F}_v) \cdot \mathbf{n} dS = \mathbf{0}, \tag{1}$$

where V is a moving control volume bounded by the surface Γ, $\mathbf{Q}$ represents a vector of the volume-averaged conservative variables, $\mathbf{n}$ is the outward unit face normal vector, and $\mathbf{F}_i$ and $\mathbf{F}_v$ are the inviscid and viscous flux vectors, respectively. Note that for a moving control volume, the inviscid flux vector must account for the difference in the fluxes due to the movement of control volume faces. Given a flux vector $\mathbf{F}$ on a static grid, the corresponding flux vector $\mathbf{F}_i$ on a moving grid is defined as $\mathbf{F}_i = \mathbf{F}\text{-}\mathbf{Q}(\mathbf{W}\cdot\mathbf{n})$, where $\mathbf{W}$ is a local face velocity.

The governing equations are closed with the perfect gas equation of state and an appropriate turbulence model for the eddy viscosity. It should also be noted that for the special case of $\mathbf{Q}=\boldsymbol{const}$, the conservation equations (1) reduce to the Geometric Conservation Law (GCL):

$$\frac{\partial V}{\partial t} + \oint_{\Gamma} \mathbf{W} \cdot \mathbf{n} dS = \mathbf{0}. \tag{2}$$

The GCL provides a precise relation between the rate of change of the time-dependent control volume and its local face velocity **W.** Though the GCL equation is a direct consequence of the governing equations (1) and is satisfied at the differential level, this is usually not the case at the discrete level. To preserve a constant solution on dynamic grids, the discrete GCL residual R_{GCL} is added to the discretized flow equations (see [1] for further details).

The 3-D URANS equations (1) are solved using a 2nd-order finite volume code, FUN3D. The code can be used to perform aerodynamic simulations across the speed range, and an extensive list of options and solution algorithms is available for spatial and temporal discretizations on general static or dynamic mixed-element unstructured grids.[1, 2] In the present study, the time derivative and contour integral in (1) are discretized using a 2nd-order backward difference (BDF2) formula and 2nd-order node-centered finite volume scheme,[2] respectively. The inviscid fluxes at

[1] Graduate student, 1601 E. Market St., Greensboro, NC
[2] Associate Professor, Department of Mathematics, 1601 E. Market St., Greensboro, NC. Senior member AIAA

cell interfaces are computed using Roe's approximate Riemann solver, and the viscous fluxes are approximated by a method equivalent to a 2nd-order finite element Galerkin procedure. The mesh velocity terms are evaluated with the BDF2 formula consistent with the discretization of the time derivative. The eddy viscosity is modeled by the one-equation turbulence model of Spalart and Allmaras.[3] The solver demonstrates high parallel scalability which is achieved through domain decomposition and message passing communication.

An approximate solution of the linear system of equations formed within each time step is obtained with a multicolor Gauss-Seidel point-iterative scheme. To accelerate the convergence, a low-Mach-number preconditioner similar to one developed in [4] is used at each time step. This preconditioning technique is briefly outlined in Section III. The turbulence model is integrated all the way to the wall without the use of wall functions and is solved separately from the mean flow equations.

II. Rigidly Moving Grid

To accurately resolve the flow near a wing during the entire flapping motion, a body-fitted mesh is regenerated at each time step, so that it moves rigidly along the wing. The rigid mesh motion is generated by a 4x4 transformation matrix.[1] The transformation matrix enables general translations and rotations of the grid according to the following relation:

$$\mathbf{X} = T\mathbf{X}_0,$$

which moves a point from an initial position (x_0, y_0, z_0) to its new position (x, y, z):

$$\begin{bmatrix} x \\ y \\ z \\ 1 \end{bmatrix} = \begin{bmatrix} r_{11} & r_{12} & r_{13} & t_x \\ r_{21} & r_{22} & r_{23} & t_y \\ r_{31} & r_{32} & r_{33} & t_z \\ 0 & 0 & 0 & 1 \end{bmatrix} \begin{bmatrix} x_0 \\ y_0 \\ z_0 \\ 1 \end{bmatrix}. \tag{3}$$

In Eq. (3), the 3x3 matrix R defines a general rotation, and the vector $\mathbf{t} = [t_x, t_y, t_z]^T$ specifies a translation. Note that the matrix T depends on time. One key feature of this approach is that multiple transformations telescope via matrix multiplication. This formulation is particularly attractive for composite parent-child body motion. Herein, the rotation associated with the wing pitching is specified relative to the flapping motion.

III. Flapping Wing Kinematics

In the present analysis, the kinematics of an idealized insect wing motion is defined as two rotations associated with the flapping and pitching motions:

$$\begin{cases} \theta = \theta_0 \sin(2\pi f_w t) \\ \alpha = \alpha_0 \sin(2\pi f_w t + \varphi) \end{cases} \tag{4}$$

where θ_0 denotes a stroke amplitude, α_0 is a pitch amplitude, f_w is a wing stroke cycle frequency, and φ is a phase shift angle between the flapping and pitching motions. The parameters θ_0, α_0, φ are set equal to 180^0, 45^0, 90^0, respectively. The rotation associated with the flapping motion occurs with respect to the wing root. The wing flips (pitches) about an axis located at 50% of the chord. The pitching axis remains in the stroke plane throughout the entire motion, and the forward and backward stroke arcs are kinematically symmetric. Note that for this wing motion, the midpoint of the flip occurs precisely at the end of the forward stroke or the end of the backward stroke.

IV. Low-Mach-number Preconditioning

Since the compressible URANS equations are used to describe the flapping wing flow at very low Mach numbers, some proper preconditioning is required to accelerate the convergence of the unsteady numerical solution at each time step. This is achieved by using a low-Mach-number preconditioner developed by Turkel and Vatsa for the unsteady Navier-Stokes equations.[4] To preserve the time-dependent behavior of the original unsteady equations, the preconditioning is incorporated into the dual-time stepping framework as follows:

$$P^{-1}\frac{\partial(V\mathbf{Q})}{\partial\tau}+\frac{\partial(V\mathbf{Q})}{\partial t}+\mathbf{R}=\mathbf{0} \tag{5}$$

where t is the physical time, τ is an artificial time, $\mathbf{R}$ is the spatial residual, $\mathbf{Q}$ is a vector of the conservative variables, P is a preconditioning matrix. At each physical time step, the first term in Eq. (5) converges to zero, thus recovering the original unsteady discrete equations and providing time-accurate numerical solution. The preconditioning matrix P is given by

$$P=\frac{\partial\mathbf{Q}}{\partial\mathbf{U}}\begin{bmatrix}\beta^2 & 0 & 0 & 0 & 0\\ 0 & 1 & 0 & 0 & 0\\ 0 & 0 & 1 & 0 & 0\\ 0 & 0 & 0 & 1 & 0\\ \dfrac{(\beta^2-1)T}{c_p p} & 0 & 0 & 0 & 1\end{bmatrix}\frac{\partial\mathbf{U}}{\partial\mathbf{Q}} \tag{6}$$

where β is a user-defined parameter which is of the order of the mean Mach number, $\mathbf{U}$ and $\mathbf{Q}$ are vectors of the primitive and conservative variables, respectively. The matrix P is constructed such that all eigenvalues of the preconditioned Jacobian matrix are of the order of one, thus eliminating the large disparity between acoustic and convective wave speeds. A detailed description of the above preconditioning technique can be found elsewhere.[4]

V. Results and Discussion

We now study the aerodynamic characteristics of a single rigid wing undergoing an insect-based flapping motion. It is assumed that the ambient flow is quiescent. The Reynolds number based on the wing chord length and the maximum wing tip velocity is 5096. The wing has a span of 2.12 cm and mean chord of 1.0 cm. The reduced flapping frequency nondimensionalized by the maximum wing tip velocity is set be 0.32, which corresponds to the flapping frequency of 34 Hz. A hexahedral body-fitted mesh with approximately 1 million cells is used in all numerical experiments. The rigidly moving body-fitted grid provides good resolution of the flow near the wing over the entire time interval considered. The outer boundary is placed 20 chord lengths away from the wing. Fifty time steps per one flapping cycle are used to resolve the wing dynamics. It is assumed that the characteristic size of a gust is much larger than that of the flapping wing. For all cases considered, no gust is initially present in the system, and the flow is quiescent. Over this initial period of time, the wing makes two full strokes, which is sufficient to remove initial transients, so that the solution reaches its quasi-periodic regime.

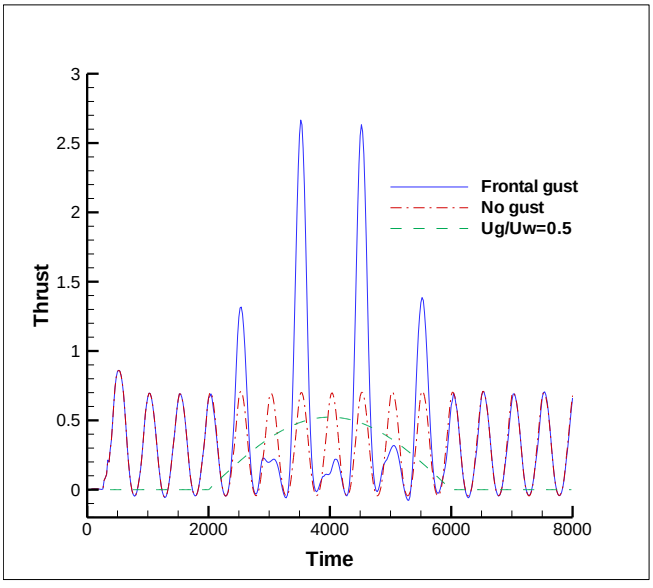

Figure 1. Time histories of the gust velocity and the wing thrust coefficient computed with and without the frontal gust.

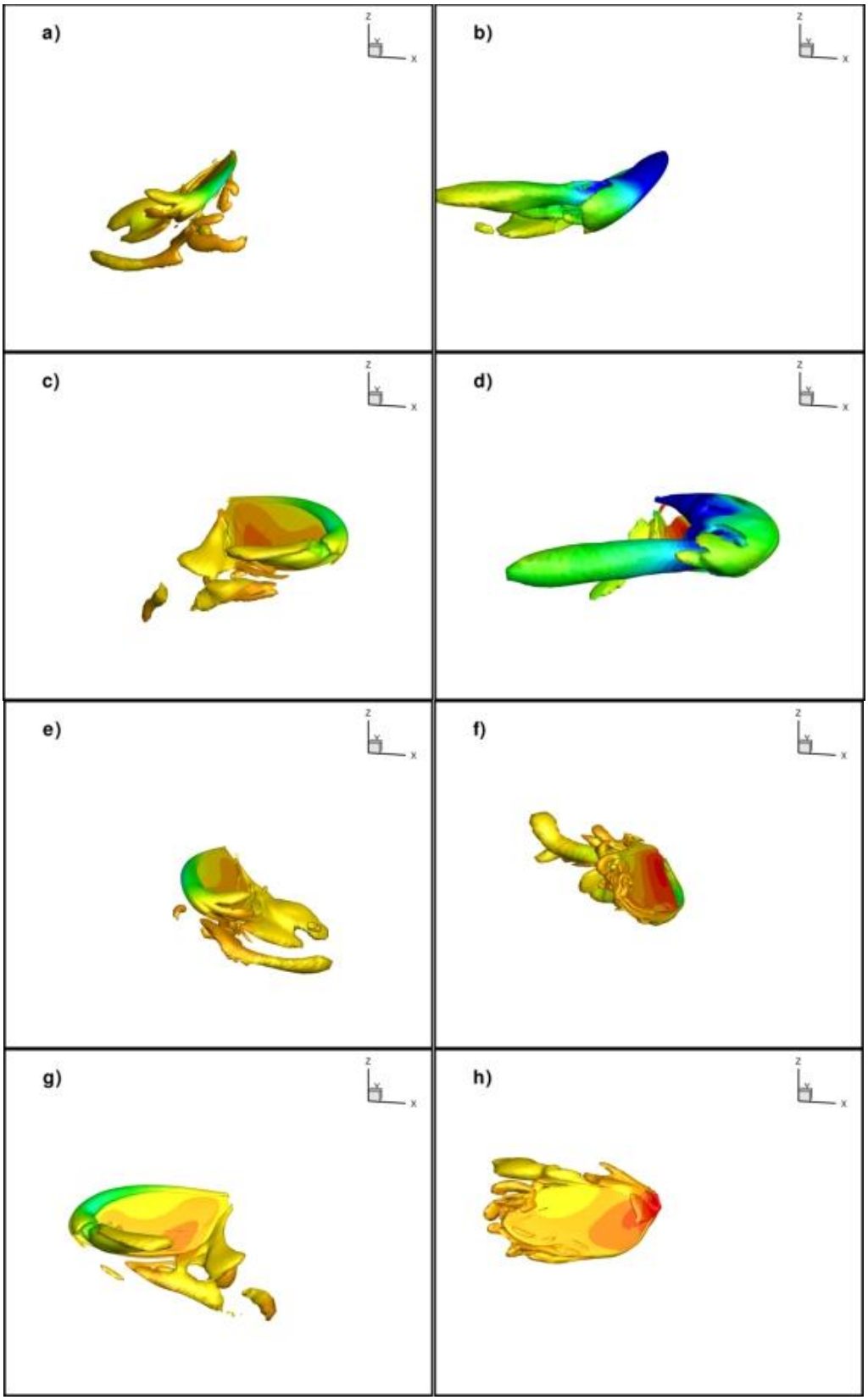

Figure 2. Snapshots of the iso-surface of the *q*-criterion colored with pressure contours at four instants in time: (a-b) t=3500, (c-d) t=3600, (e-f) t=4000, (g-h) t=4100, obtained with (right column) and without frontal gust.

A. Frontal gust

First, we analyze the response of the flapping wing to a frontal wind. The wind gust velocity is oriented along the *x*-axis, i.e. $[U_g, 0, 0]^T$, where

$$U_g(t) = \begin{cases} U_0 \sin(2\pi f_g t), \text{for } t_b \le t \le t_e \\ 0, \qquad \text{otherwise} \end{cases}$$

The gust frequency f_g is set to be 4 times less than the wing flapping frequency, f_w. As a result, the wing makes 4 full strokes during the wing gust. The gust velocity amplitude U_0 is set equal to one half of the maximum wing tip velocity. Figure 1 shows time histories of the thrust coefficient obtained with and without the frontal wing gust. As follows from this comparison, the frontal gust has a very strong effect on the instantaneous thrust generated by the flapping wing. In the presence of the wind gust, the maximum peak value of the thrust coefficient during the forward stroke is more than two times larger than that in the quiescent air. This behavior reverses during a backward stroke when the thrust drops down to the level which is less than half of its value under the quiescent flow condition. These large variations in the peak values of the thrust coefficient are directly related to variations in strength of the leading edge vortex, as one can see in Fig. 2. Indeed, the wing moves against the wind gust during the forward stroke. As a result, the relative wing velocity significantly increases as compared with its baseline value obtained in the hovering case where no gust is present. This increase in the relative wing velocity results in generation of a much stronger leading edge vortex during the forward stroke, as seen in Figs. 2a-2d. The strengthening of the leading edge vortex increases the pressure difference between the windward and leeward sides of the wing, thus increasing the thrust. During the backward stroke, the wing comes along with the gust, so that the relative wing velocity with respect to the wind gust is reduced as compared with that in the quiescent flow. Figures 2e-2h show that the leading edge vortex generated during the backward stroke in the presence of the wind gust is much weaker than its strength in the quiescent flow. Another important observation is that the wind gust significantly reduces the wake capture effect, in which the wing passes through the vortex shed in the previous stroke, as one can see in Fig. 2b and 2f.

B. Downward gust

We now consider the effect of a short duration downward wind gust on the flapping wing performance. All wing and gust parameters are kept the same as in the previous case except that the wind gust velocity is now oriented vertically in the downward direction with respect to the *xy*-plane in which the flapping motion occurs. Figure 3 shows time histories of the thrust coefficient obtained in the quiescent air and in the presence of the wing gust. The mean thrust coefficient gradually decreases as the wing gust velocity increases and achieves its minimum value when the gust velocity is the highest. During this period of time, the time-averaged (over each flapping cycle) wing thrust coefficient becomes negative, thus indicating that the flapping wing is strongly susceptible to downward gust even if its amplitude is quite moderate and equal to one half of the wing tip velocity. This drastic reduction in the trust coefficient is mainly due to weakening of the leading edge and root vortices, as is evident from Fig. 4.

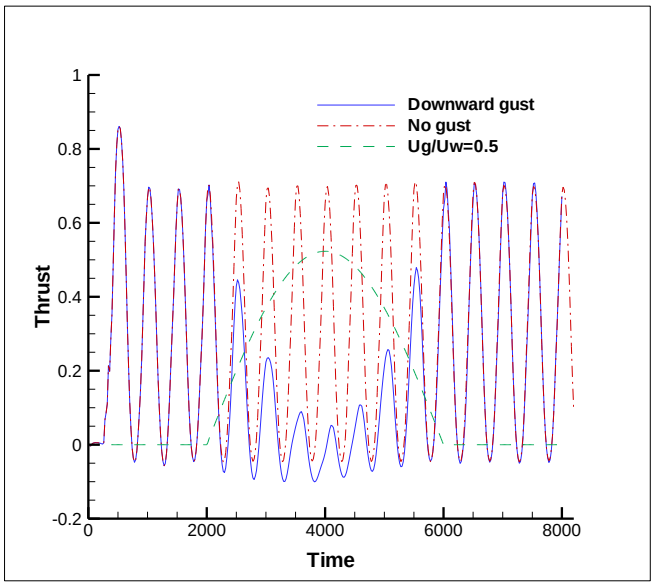

Figure 3: Time histories of the gust velocity and the wing thrust coefficient computed with and without downward gust.

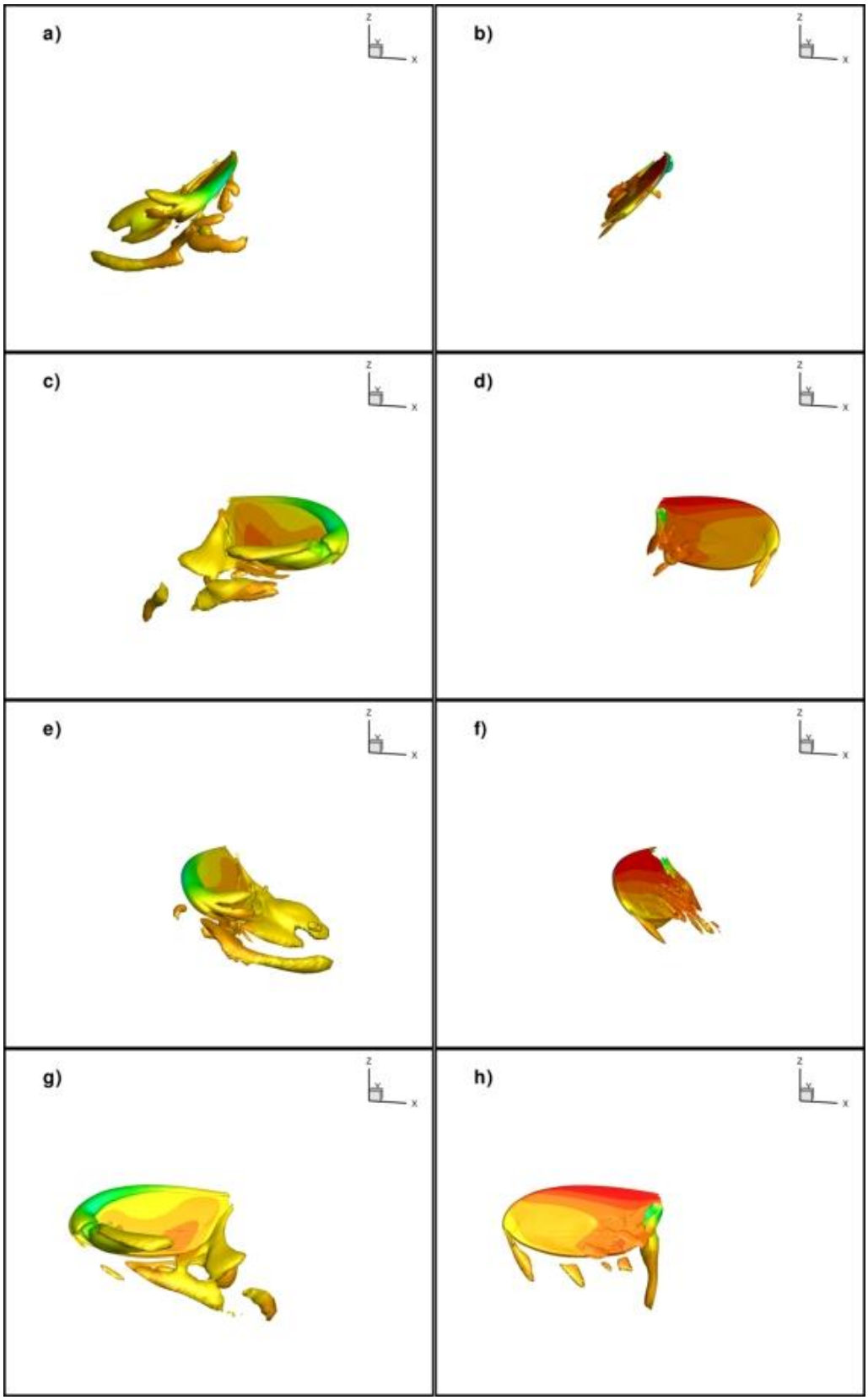

Figure 4. Snapshots of iso-surface of the *q*-criterion colored with pressure contours at four instants in time (a-b) t=3500, (c-d) t=3600, (e-f) t=4000, (g-h) t=4100, obtained with (right column) and without downward gust.

As the downward gust velocity increases, the strength of the leading edge vortex decreases. This behavior can be explained by the fact that the effective angle of attack of the wing with respect to the total flow velocity vector reduces as the gust velocity increases. Another mechanism that contributes to the reduction of the thrust coefficient is that the leading edge vortex shed during the previous stroke is convected downward by the wind gust, thus practically eliminating the wake capture effect when the gust velocity reaches its maximum value, as one can see in Fig. 4b and 4f. Another conclusion that can be drawn from these studies is that the thrust coefficient returns to its baseline profile after one flapping cycle once the wind gust is removed. It gives us an indication that the flapping wing effectively recovers from wind gust fluctuations and demonstrates the potential for providing a stable flight in gusty environment.

C. Side gust

The last case concerns the influence of a side gust on the performance of the same hovering wing considered in the previous two cases. The gust starts during the 2nd wing stroke and increases sinusoidally, reaching its maximum value during the 4th stroke. As in the previous cases, the wing makes 4 full strokes during the wind gust, and the ratio of the gust velocity to the maximum wing tip velocity is equal to 0.5, which corresponds to the gust amplitude of approximately 3.5 m/s. Time histories of the flapping wing thrust coefficient computed with and without the

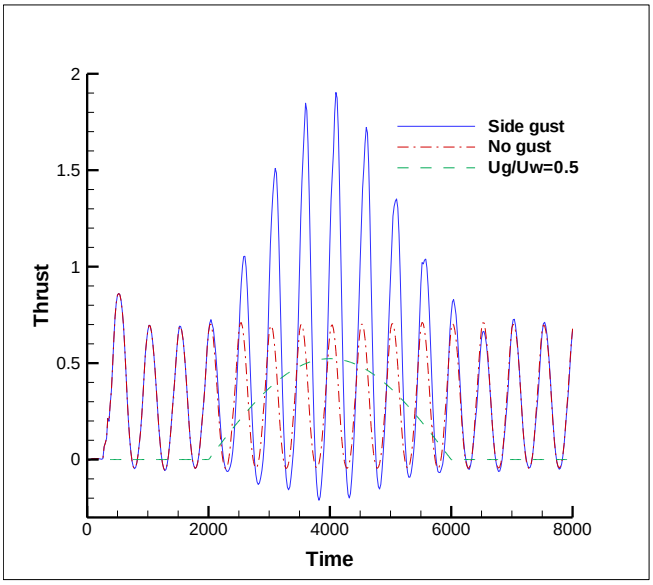

Figure 5: Time histories of the wind gust velocity and the thrust coefficient of a flapping wing with and without side gust.

presence of the side gust are shown in Fig. 5. As one can see in the figure, the time-averaged thrust coefficient grows as the gust velocity increases. The highest peak value of the thrust coefficient occurs near t=4000 when the gust velocity reaches its maximum. Similar to the downward- and frontal-gust cases, the response time of the flapping wing to the side wind gust is much shorter than one flapping cycle. It should also be noted that when the gust wind is the strongest, the thrust generated by the wing becomes negative over a small portion of the full stroke. Despite these large variations in thrust, the time-averaged (over each flapping cycle) thrust coefficient varies not so significantly over its mean value, thus indicating that the flapping wing maintains a stable thrust under the moderate side wind conditions. To gain a deeper insight into the flow physics of the flapping wing in the presence of side gust, snapshots of an isosurface of the q-criterion obtained with and without gust are presented in Fig. 6. The q-criterion reveals the rotational flow regions, thus identifying the leading edge, root, and tip vortices. As follows from Fig. 6, the presence of the side wind gust strengthens the leading edge and tip vortices during both the forward and backward strokes. Another important observation is that the vortex shed from the wing leading edge in the previous backward or forward stroke is convected towards the wing by the side gust. These additional vortices influence the flowfield during the next stroke, thus increasing the amplitude of oscillations of the thrust coefficient.

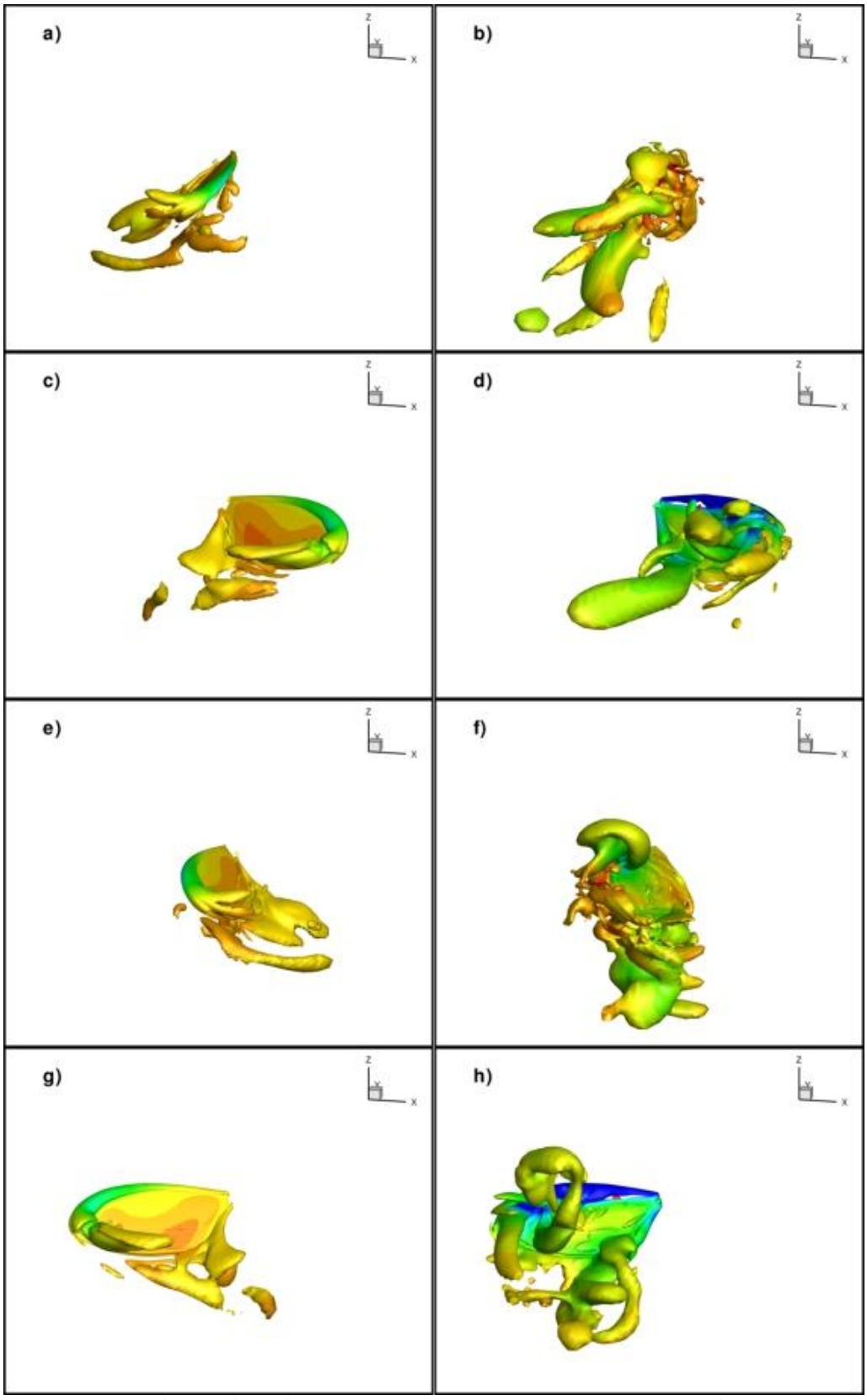

Figure 6. Snapshots of iso-surface of the *q*-criterion colored with pressure contours at four instants in time (a-b) t=3500, (c-d) t=3600, (e-f) t=4000, (g-h) t=4100, obtained with (right column) and without side gust.

VI. Conclusions

The performance of a flapping wing under various gust conditions including frontal, downward, and side gusts has been studied using the 3-D fully unstructured, unsteady RANS code, FUN3D. As follows from our numerical results, the downward gust drastically reduces the thrust generated by a centimeter-scale flapping wing when the ratio of the gust velocity to the wing tip velocity is 0.5, thus indicating that small-scale flapping-wing MAVs may be susceptible to downward gusts. In the case of a frontal gust of the same amplitude used in the downward case, the peak value of the wing thrust coefficient during the forward (with respect to the wind direction) stroke exceeds its baseline value by more than a factor of 2. This increase in thrust is compensated by a similar reduction during the backward stroke, thus leading to no appreciable changes in the time-averaged thrust coefficient. A moderate increase in the time-averaged thrust coefficient is observed in the case of the side gust which has only a marginal effect on the flapping wing performance. These results indicate that flapping-wing MAVs can alleviate the frontal and side gust effects if the mean gust velocity is less or comparable with the wing tip velocity. Another interesting observation is that for all types of gusts, the thrust generated by the flapping wing returns to its baseline profile over just one full stroke once the gust is removed, thus showing that the flapping wing can effectively recover from wind gust fluctuations.

Acknowledgments

This work was supported by the MAST CTA Center for Microsystem Mechanics sponsored by Army Research Laboratory.

References

1. Biedron, R.T. and Thomas, J.L., "Recent Enhancements to the FUN3D Flow Solver for Moving Mesh Applications," AIAA 2009-1360, 2009.
2. Anderson,W. K., and Bonhaus, D. L., "An Implicit Upwind Algorithm for Computing Turbulent Flows on Unstructured Grids," *Computers and Fluids*, Vol. 23, No. 1, 1994, pp. 1–21.
3. Spalart, P.R. and Allmaras, S.R., "A One-Equation Turbulence Model for Aerodynamic Flows," AIAA Paper 92-0439, 1991.
4. Turkel, E. and Vatsa,V.N., "Choice of variables and preconditioning for time dependent problems," AIAA Paper 2003-3692, 2003.